NASA

Technical Memorandum 84000

Anisotropy in MHD Turbulence Due to a Mean Magnetic Field

J. V. Shebalin, W. H. Matthaeus, and D. Montgomery

SEPTEMBER 1982

National Aeronautics and Space Administration

Goddard Space Flight Center
Greenbelt, Maryland 20771

ANISOTROPY IN MHD TURBULENCE DUE TO A MEAN MAGNETIC FIELD

John V. Shebalin†
Westinghouse Electric Corporation
Oceanic Division
Annapolis, Maryland 21404, U.S.A.

William H. Matthaeus*
NASA/Goddard Space Flight Center
Greenbelt, Maryland 20771, U.S.A.

and

David Montgomery*
University of Maryland
College Park, Maryland 20742, U.S.A.

† Present address: Kentron Technical Center, Hampton, Virginia 23666.

* Permanent address: College of William and Mary, Williamsburg, Virginia 23185.

ABSTRACT

The development of anisotropy in an initially isotropic spectrum is studied numerically for two-dimensional magnetohydrodynamic turbulence. The anisotropy develops due to the combined effects of an externally imposed dc magnetic field and viscous and resistive dissipation at high wave numbers. The effect is most pronounced at high mechanical and magnetic Reynolds numbers. The anisotropy is greater at the higher wave numbers.

1. Introduction

In the last several years, a systematic theory of magnetohydrodynamic (MHD) turbulence has developed, but it has dealt largely with the case in which no mean dc magnetic field is present. The presence of a mean dc magnetic field renders MHD turbulence inherently anisotropic, and one can no longer take advantage of the contraction of the statistical description that the isotropy provides. Here, we report a beginning on the problem of describing MHD turbulent phenomena in the presence of the anisotropy introduced by a mean dc magnetic field. We proceed numerically, using a two dimensional, spectral-method, incompressible MHD code which has been modified to include the presence of a mean dc magnetic field.

It would, of course, have been preferable to have used three-dimensional numerics. However, codes with adequate resolution to study three dimensional MHD turbulence at high mechanical and magnetic Reynolds numbers are rare, and groups with adequate computer resources to study MHD turbulence with them systematically are rarer still. It has been possible to represent in two dimensions several of the features which we believe to be central to the three dimensional case.

There are relatively few published results of laboratory measurements of MHD turbulence. Five important papers are due to Robinson, Rusbridge, and Saunders (1968), Rusbridge (1969), Robinson and Rusbridge (1971), Zweben, Menyuk and Taylor (1979), and Zweben and Taylor (1981). The first three of these report measurements on the Culham-Harwell ZETA toroidal Z-pinch, and the last two, measurements on the UCLA Macrotor Tokamak. The most important two features that emerged from the magnetic fluctuation measurements on both machines were: (1) the single-point frequency spectra were broad-band, extending from a few hundred kiloherz down to the lower limit of the frequency resolution, with a

notable absence of spikes or peaks; and (2) the wave-number spectra were peaked sharply in the direction perpendicular to the mean field, which manifested itself as a large ratio of parallel to perpendicular correlation lenghts (≥ 10). Both of these behaviors will be seen below to emerge from the evolution of initially isotropic spectra in two dimensions.

The presence of a similar anisotropy is essential, in one form or another, to a theoretical derivation of the Strauss equations (Strauss 1976, Montgomery 1982). The Strauss equation are a reduced set of MHD equations, intermediate between two and three dimensions, which have found wide applicability to tokamak dynamics and may have considerably broader utility. It is unclear how to proceed in their derivation if the strong anisotropy is not present initially, and it would be reassuring to know that an initially isotropic spectrum would relax to an appropriately anisotropic one.

The code used here has evolved from the spectral-method techniques given by Orszag (1971) and Patterson and Orszag (1971). Fyfe, Joyce, and Montgomery (1977a,b) and Matthaeus and Montgomery (1980, 1981) have used earlier versions of the present code to study forced dissipative MHD turbulence, selective decay processes, and the evolution of the sheet pinch, all in the presence of periodic boundary conditions. Orszag and Tang (1979) have used a similar code to study small scale effects in two dimensions, and Pouquet (1978) has reported closure calculations for the same geometry. A general review of two dimensional turbulence has been given by Kraichnan and Montgomery (1980). None of the above work addresses the case of a finite mean dc magnetic field.

The outline of this present paper is as follows. In § 2, the dynamical equations are described: they are only a slight modification of those used previously. The computational technique is briefly remarked upon

in § 3. Results from the computations are presented in § 4, 5, and 6. The most important effect consistently observed is the development of strong anisotropy in the spectra from isotropic initial conditions. The anisotropy develops towards the kinds of spectra which seem to prevail in the reported measurements in ZETA and Macrotor. The development of the anisotropy depends upon the combined effect of the external dc magnetic field strength and the size of the Reynolds numbers in an unexpected, but ultimately simple, way. A simple model of the effect is offered in § 7, where the results are briefly summarized and further directions for research are indicated.

2. Dynamical Equations

The incompressible, dissipative MHD equations in two dimensions are used. The magnetic field consists of a constant mean field part $\underset{\sim}{B}_o = B_o\hat{e}_x$, plus a time-dependent zero-mean turbulent part $\underset{\sim}{B} = (B_x, B_y, 0) = \nabla x(\hat{e}_z a)$. The magnetic vector potential is $\hat{e}_z a(x, y, t)$ so that the Coulomb gauge is employed. For all variables, $\partial/\partial z \equiv 0$. The velocity field $\underset{\sim}{v} = (v_x, v_y, 0) = \nabla x(\hat{e}_z \psi)$ is expressed in terms of a stream function $\psi = \psi(x, y, t)$ and has zero mean. In what has become a standard set of dimensionless variables, the vorticity $\underset{\sim}{\omega} = \omega\hat{e}_z = \nabla x \underset{\sim}{v}$, so that $\omega = -\nabla^2\psi$. Similarly, the electric current $\underset{\sim}{j} = j\hat{e}_z$, with $\nabla^2 a = -j$.

Magnetic fields are measured in terms of the initial root mean square turbulent field strength B. Velocities are measured in units of the Alfvén speed corresponding to B. The dimensionless viscosity and resistivity ν and η are the reciprocals of mechanical and magnetic Reynolds numbers, respectively. The simplest form of the dynamical equations is, in the two-dimensional geometry,

$$\frac{\partial \omega}{\partial t} + \underset{\sim}{v}\cdot\nabla\omega = \underset{\sim}{B}\cdot\nabla j + \nu\nabla^2\omega + B_o\frac{\partial j}{\partial x} \qquad (1)$$

and

$$\frac{\partial a}{\partial t} + \underset{\sim}{v}\cdot\nabla a = \eta\nabla^2 a + B_o\frac{\partial \psi}{\partial x} . \qquad (2)$$

Without the B_o terms, eqs. (1) and (2) become those considered previously. In a recent derivation (Montgomery, 1982), the Strauss (1976) equations were re-derived using a perturbation expansion of the full set of incompressible MHD equations in three dimensions, in powers of B/B_o. It was necessary to assume in the derivation that the time derivatives $\partial/\partial t$ remained of O(1), or that no zeroth-order population of Alfvén waves was present. (The

linearized solutions for the three-dimensional case, as for eqs. (1) and (2), is just a superposition of Alfvén waves with angular frequencies $\omega(\underset{\sim}{k}) = \pm \underset{\sim}{k} \cdot \underset{\sim}{B}_o$, where $\underset{\sim}{k}$ is the wavenumber.) An objective of the present computation is to see how a spectrum evolves which does contain an initially isotropic spectrum of Alfvén waves. It will be shown that the spatial dependence of such a spectrum on the parallel spatial coordinate x becomes progressively relatively weaker with time.

3. Computational Technique

The essence of the computational method is that all physical fields are expanded in truncated Fourier series. The Fourier coefficients are stepped forward in time and are saved at predetermined time steps to provide a history of the dynamical evolution of the field variables. To be explicit, Fourier representations of ω and a (for example) are (see, e.g., Fyfe et al, 1977a, b):

$$\omega(\underset{\sim}{x},t) = \Sigma_{\underset{\sim}{k}}\omega(\underset{\sim}{k},t)\exp(i\underset{\sim}{k}\cdot\underset{\sim}{x}) \tag{3}$$

$$a(\underset{\sim}{x},t) = \Sigma_{\underset{\sim}{k}}a(\underset{\sim}{k},t)\exp(i\underset{\sim}{k}\cdot\underset{\sim}{x}), \tag{4}$$

where $\underset{\sim}{k} = (k_x, k_y)$ and k_x and k_y are integers. Thus the dimension of the square box is chosen for convenience to be 2π. The Fourier coefficients retained lie in the range $k_{min} = 1 \leq |\underset{\sim}{k}| \leq k_{max}$, where k_{max} is essentially limited by available computer time. Limitations on the Reynolds numbers are provided by the requirements that ν and η be large enough so that the Fourier coefficients for $|\underset{\sim}{k}| \geq k_{max}$ are suppressed.

The first test of the code was to run it with the dissipative terms removed. Conservation laws can then be tested and comparisons can be made between the computed behavior of the Fourier coefficients and the predictions of the (unphysical) absolute equilibrium ensemble theory (see, e.g., Kraichnan and Montgomery, 1980).

The second step was to compare dissipative results from two runs, both having twice the other's value of k_{max}, and thus having twice the spatial resolution. The third step was to run several cases with varying values for ν and η at a particular value of B_o, to determine the influence of the Reynolds

numbers. Finally, the last step was to run a number of cases which differed only in the value of B_o, thereby investigating the effect that varying mean magnetic field strength has on the dynamics.

Initial Fourier coefficients were chosen so that they would be non-zero only within a given annulus in $\underset{\sim}{k}$-space. The $\omega(\underset{\sim}{k},t)$ were initially non-zero only for $k_1 \leq k \leq k_2$, and the $a(\underset{\sim}{k},t)$ were non-zero only for $k_3 \leq k \leq k_4$. Within their respective annuli, the values of the $\omega(\underset{\sim}{k},0)$ were chosen so that all $|\underset{\sim}{v}(\underset{\sim}{k},0)| = |\omega(\underset{\sim}{k},0)|/k$ were equal, and the $a(\underset{\sim}{k},0)$ were chosen so that all $|\underset{\sim}{B}(\underset{\sim}{k},0)| = k|a(\underset{\sim}{k},0)|$ were equal. The phases of the $a(\underset{\sim}{k},0)$ and $\omega(\underset{\sim}{k},0)$ were assigned randomly. The specification of the initial Fourier coefficients was completed by giving values for the magnetic energy $E_B \equiv \Sigma_{\underset{\sim}{k}}|\underset{\sim}{B}(\underset{\sim}{k},t)|^2/2$ and the kinetic energy $E_v \equiv \Sigma_{\underset{\sim}{k}}|\underset{\sim}{v}(\underset{\sim}{k},t)|^2/2$ at $t = 0$.

The total energy is $E \equiv E_B + E_v$, the "cross helicity" is $P \equiv \Sigma_{\underset{\sim}{k}}\underset{\sim}{v}(\underset{\sim}{k},t)\cdot\underset{\sim}{B}^*(\underset{\sim}{k},t)/2$. The mean square vector potential is $A \equiv \Sigma_{\underset{\sim}{k}}|a(\underset{\sim}{k},t)|^2/2$. E, P, and A are significant quantities in the theory of two dimensional MHD turbulence in the absence of a mean field: they are the only known non-dissipative invariants which remain invariant under truncation of the Fourier-expanded ($\nu = 0 = \eta$) version of eqs. (1) and (2) with $B_o = 0$. If $B_o \neq 0$, E and P still have this status, but A does not. We may define $R \equiv E_B/E_v$ as the ratio of the energies.

About a dozen different sets of initial Fourier coefficients have been used for various runs. Many of the sets exhibited similar behavior. The number of different sets of initial conditions presented in this paper has been kept to a minimum, but for the runs discussed, there are others unreported for which the behavior was similar. Details of the runs explicitly discussed here are collected in Tables 1 and 2.

4. Non-dissipative Tests

To test the spectral code, several cases were run with $\nu = \eta = 0$, and the results compared with absolute equilibrium ensemble theory. Such results are, of course, unphysical, and should be regarded as preliminary to the dissipative results presented in § 5.

Equilibrium ensemble theory for the $B_o = 0$ case was given by Fyfe and Montgomery (1976); the case $B_o \neq 0$ is recovered by simply deleting the third "rugged" constant of the motion A. The prediction is a simple equipartition, $\langle|\underset{\sim}{v}(\underset{\sim}{k})|^2\rangle = \langle|\underset{\sim}{B}(\underset{\sim}{k})|^2\rangle = \text{const.}$, independently of $\underset{\sim}{k}$. This is true for all realizable values of $\langle E\rangle$ and $\langle P\rangle$. The ratio $\langle R\rangle \equiv \langle E_B\rangle/\langle E_v\rangle = 1$, in sharp contrast to the $B_o = 0$ case. There is no crowding to the long wavelengths as $k_{max} \to \infty$, as there is when $B_o = 0$.

Non-dissipative computations were carried out with $B_o = 0$ and $B_o = 1$ for different sets of initial coefficients. Time averages were made of phase functions of the Fourier coefficients and these were compared with ensemble averages. The two should be equal to the extent that the system is ergodic.

The results of a single set of Fourier coefficients will be presented here, call it set A. For run A1, $B_o = 0$, and for run A2, $B_o = 1$. For both runs, $k_{max} = 16$, $E = 1.0$, the time step was $(256)^{-1}$. The total number of time steps was 12,800. For these conditions, $k_1 = k_3 = 3$ and $k_2 = k_4 = 5$. Time averages were performed over the last 11,520 time steps.

The comparison between the numerical results and the ensemble predictions is given in Table 1 and in Figures 1 through 4. In Table 1, the behavior of E, P, A, and the evolving ratio $R_t \equiv E_B/E_v$ is shown as a function of time. The invariants E, P, and A for $B_o = 0$ and E and P for $B_o = 1$ are conserved to a few percent in all cases. Non-dissipative runs for initial conditions "B"($E_B = E_v = 1$, $k_1^2 = 5$, $k_2^2 = 8$, $k_3^2 = 10$, $k_4^2 = 13$) will not be reported in detail.

In Figs. 1 through 4, the directionally averaged magnetic and kinetic modal energies are presented for time averaged data. (Directional averaging means averaging over all values of $\underset{\sim}{k}$ corresponding to a particular k^2.) At the lower values of k, where the number of degenerate $\underset{\sim}{k}$'s is sparse, occasionally large anisotropies necessarily appear, but no systematic directionality was observed. An explicit comparison of these runs with corresponding dissipative runs will be presented in the next section, after suitable measures of anisotropy are defined. It will be seen that the non-dissipative runs, in contrast to the dissipative ones, show no anisotropy when averaged over long times.

In Figs. 1 through 4, the spectral predictions of the absolute equilibrium ensemble theory are shown as solid lines and the plotted points are the time-averaged results of the computations. No significant departures from the predictions of the absolute equilibrium ensemble theory have been observed in these runs, and in others not reported here. Typical behavior for almost all the individual Fourier modes (those with $k_x \neq 0$) is that of an Alfvén wave of angular frequency $\omega(\underset{\sim}{k}) = \pm \underset{\sim}{k} \cdot \underset{\sim}{B}_o$. This is the principal qualitative difference in the time behavior observed between the $B_o = 0$ and $B_o \neq 0$ cases. Superposed on the Alfvén-wave oscillations is a slower transfer of excitation between the Fourier modes.

In the next few sections, we pass to a consideration of the dissipative cases. In order to maintain a common thread throughout the discussion, we will primarily use set A as the initial conditions for the dissipative runs to be presented. The principal quantities to be varied are the spatial resolution k_{max}, the values of the dissipation coefficients ν and η, and the external field strength B_o.

5. Appearance of Anisotropy: Effects of Viscosity, Resistivity, and Spatial Resolution

In this section, we describe dissipative runs. The presence of dissipation is always central in the evolution of any real turbulent field.

We use primarily the same initial Fourier coefficients as those in § 4. The most striking effect we have observed is that when both dissipation and a mean B_o are present, anisotropy appears. The $\underset{\sim}{k}$ spectrum evolves into one peaked perpendicularly to the mean field $\underset{\sim}{B}_o$. We describe the dependence of this anisotropy on the dissipation coefficients and the mean B_o, after first remarking upon some considerations of necessary spatial resolution.

For an accurate solution to eqs. (1) and (2), we must resolve the smallest dynamically significant spatial scales that ν and η permit. An estimate for these is provided by the Kolmogoroff "dissipation wave number", constructed by dimensional analysis based on the rate of dissipation of energy. For MHD in two dimensions, it is

$$k_d = [\eta^{-3}|dE_B/dt|_\eta + \nu^{-3}|dE_v/dt|_\nu]^{1/4}, \qquad (5)$$

where $|dE_B/dt|_\eta$ and $|dE_v/dt|_\nu$ are the ohmic and viscous energy dissipation rates, respectively. Ideally, k_d should be less than k_{max} for accurate solution of eqs. (1) and (2) and this provides at present the most severe limitation on turbulence computations, both Navier-Stokes and MHD. For some purposes, it may be that when the smallest scales are dynamically insignificant, k_d somewhat larger than k_{max} may be tolerated, but $k_d >> k_{max}$ must always signal uselessness in a turbulence computation. Other measures of mean length scales for the turbulent field, such as those of Pao and Taylor (see, e.g., Leslie 1973) may be used to characterize turbulent activity, but the Kolmogoroff scale is the one most widely accepted and we shall use it hereafter.

The dissipation wave number may be adjusted empirically, for a given set of initial Fourier coefficients, by raising ν and η until the computed k_d remains no greater than k_{max}. We consider here only the case $\nu = \eta$ (unit magnetic Prandtl number).

In the initial set of dissipative cases, there are six runs (A3 through A8, see Table 2), having $B_o = 0$ and $B_o = 1$ for $\nu = \eta = 0.005$, 0.01 and 0.02. The following characteristics were common to these six runs: $k_{max} = 32$, time step = $(256)^{-1}$, total number of time steps = 1280, initial Fourier coefficients: set A. The temporal evolution of the variables E, P, A, and R_t for the runs with $\nu = \eta = 0.01$ are shown in figures 5 and 6. (Qualitatively similar behavior was observed for $\nu = \eta = 0.005$ and 0.02, the decay times simply increased and decreased, respectively.)

When $B_o = 0$, roughly twice as much magnetic as kinetic energy develops; when $B_o = 1$, the ratio remains approximately unity. E, P, A all monotonically decay for $B_o = 0$, but when $B_o = 1$, A actually increases at times, but overall decays.

To measure anisotropy in the $\underset{\sim}{k}$ spectrum, a set of angles were defined for each Fourier-decomposable field,

$$\theta_Q \equiv \tan^{-1}\{[\Sigma_{\underset{\sim}{k}} k_y^2 |Q(\underset{\sim}{k},t)|^2 / \Sigma_{\underset{\sim}{k}} k_x^2 \, Q(\underset{\sim}{k},t)|^2]^{1/2}\} \qquad (6)$$

where Q is any one of the fields ψ, $\underset{\sim}{v}$, ω, a, $\underset{\sim}{B}$, or j. For a $\underset{\sim}{k}$ spectrum purely normal to $\underset{\sim}{B}_o$, θ_Q is 90°, and for an isotropic spectrum, 45°.

Temporal evolution of the angles for $B_o = 0$ and $B_o = 1$ is illustrated, for runs A5 and A6, in Figs. 7 and 8, which both refer to $\nu = \eta = 0.01$. For $B_o = 0$, the angles roam unsystematically about 45°, indicating isotropic development. The anisotropy in Fig. 8, for $B_o = 1$, is typical. Notice that

the angles tend to increase in the following order: $\theta_\psi < \theta_v < \theta_\omega$, and $\theta_a < \theta_B < \theta_j$: the anisotropy is most pronounced at the shorter wavelengths. Also, when we consider $\nu = \eta = 0.005$ and 0.02 as well, we see that the degree of anisotropy tends to decrease with increasing ν and η. The results are summarized in Table 3, which displays averages of the θ_Q for $\nu = \eta = 0.005$, 0.01, and 0.02 between times 1.5 and 5.0.

Also calculated were the dissipation wave number k_d (eq. (6)), mean square vorticity $\Omega = \Sigma_{\underset{\sim}{k}} |\omega(\underset{\sim}{k},t)|^2$, and mean square current $J = \Sigma_{\underset{\sim}{k}} |j(\underset{\sim}{k},t)|^2$; the latter two quantities are required to evaluate eq. (6). The temporal evolution of Ω and J for runs A5 and A6 ($\nu = \eta = 0.01$) is shown in Fig. 9. Table 4 displays the maximum values of k_d, Ω, and J for the six runs A3 through A8. In Table 4, it is apparent that the maximum dissipation wave number decreases with increasing ν and η, as do the maxima of J and Ω. The presence of a finite B_o also apparently enforces a more nearly equal partition of dissipation between Ω and J.

From the foregoing results, it is clear that the maximum k_d which will fit inside the resolution $k_{max} = 32$ occurs for runs A5, A6, where $\nu = \eta = 0.01$. To test the effect of lowering the resolution below k_{max} on the results of runs A5 and A6, runs A9 and A10 were made with identical parameters to A5 and A6, but with $k_{max} = 16$. (We also showed that halving k_{max} allowed doubling the time step.) In runs A9 and A10, the time histories of the angles θ_Q and the quantities k_d, Ω, and J were essentially the same as those for A5 and A6 (see Shebalin, 1982, for further details). This insensivity to halving the spatial resolution, so that k_{max} falls well inside k_d, gives us some confidence in the validity of the results of such runs at the higher Reynolds numbers, such as runs A3 and A4, where k_{max} lies outside k_d.

We should remark at this point on the question of the anisotropy of the non-dissipative runs. In Fig. 10, we display the evolution of the angles θ_v and θ_B for a dissipative run B2 ($\nu = \eta = 0.0025$). Both runs have the same initial Fourier coefficients with $k_1^2 = 5$, $k_2^2 = 8$, $k_3^2 = 10$, $k_4^2 = 13$; $E_B = E_v$ for both runs, and the non-vanishing Fourier coefficients have equal amplitudes within their respective annuli, and random phases. (See Table 2.)

Referring to Fig. 10, we can see that for B1, although θ_v and θ_B initially rise to about 51° and 55° respectively, they subsequently fall and oscillate about 45°. Run B2 , however, shows θ_v and θ_B rising to maxima of approximately 66° and 68°, respectively, and then oscillating near those values. At the beginning of the dissipationless run, there apparently is a tendency toward anisotropy which cannot maintain itself; the $\nu = \eta = 0.0025$ run remains strongly anisotropic, however. This behavior, involving the necessity of small but finite dissipation in the maintenance of anisotropy, corresponds, we believe, to a simple physical effect which is discussed in § 7. It is our belief that no long-time anisotropy is to be expected without the presence of dissipation, and (for reasons given in § 7) that the smaller the dissipation coefficients, the greater the degree of anisotropy is likely to be. A computation which could afford the spatial resolution to resolve significantly higher values of k_d than we can resolve would see proportionately higher degrees of anisotropy, we believe.

6. Effects of Variable Mean Field Strength

Having discussed the effects of the spatial resolution k_{max} and the dissipation coefficients ν and η on the results, we pass to a consideration of the effects of varying the mean field B_o. Set A is chosen for the initial Fourier coefficients, and $k_{max} = 16$. Thus the runs in this section are initially similar to A9 and A10, except that B_o takes on the values 1/16, 1/8, 1/4, 1/2, 2, 4. 8, and 16. These values correspond to runs A11 through A18, respectively. (Parameters for all runs considered appear in Table 2.)

Rather than display a multitude of graphs similar to those presented for runs A9 and A10, we display mainly graphs of time averaged angles θ_Q. In Fig. 11, we show θ_Q, averaged over times 1.5 to 5.0, as functions of B_o. In Fig. 12, we show, as functions of B_o, the maximum value of k_d, the time when this maximum occurs, the maximum enstrophy Ω, and the maximum mean square current J.

Figures 11 and 12 illustrate a number of interesting effects. First, there is anisotropy which develops as B_o increases from zero. Second, the effect saturates: beyond a value of B_o of about 2, further increase in B_o results in no further increase in anisotropy, for these values of k_{max}, ν, and η. Third, the values of Ω and J approach each other as B_o increases, reflecting a progressively more Alfven-wave-like behavior at the dissipation scales. The anisotropy continued to be most pronounced at the highest wave numbers: θ_ω and θ_j were larger than the other angles.

A physical feeling for the configuration-space manifestations of the anisotropy may be obtained from Fig. 13. There, contour plots are given for the vorticity $\omega(\underset{\sim}{x},t)$ and current $j(\underset{\sim}{x},t)$ at various times with a zero and a non-zero value of B_o. For the plot in which $B_o = 2$ it is clear that, at

time t = 2.0, the vorticity and current contours have elongated in the direction of the mean field, reminiscent of the elongations that were reported in the ZETA and Macrotor devices.

7. Discussion

The linearized MHD equations in two and three dimensions result from discarding the right hand sides of

$$\frac{\partial \underset{\sim}{v}}{\partial t} - \underset{\sim}{B}_o \cdot \nabla \underset{\sim}{B} - \nu \nabla^2 \underset{\sim}{v} = \underset{\sim}{B} \cdot \nabla \underset{\sim}{B} - \underset{\sim}{v} \cdot \nabla \underset{\sim}{v} - \nabla p \tag{7}$$

and

$$\frac{\partial \underset{\sim}{B}}{\partial t} - \underset{\sim}{B}_o \cdot \nabla \underset{\sim}{v} - \eta \nabla^2 \underset{\sim}{B} = \underset{\sim}{B} \cdot \nabla \underset{\sim}{v} - \underset{\sim}{v} \cdot \nabla \underset{\sim}{B}, \tag{8}$$

subject to $\nabla \cdot \underset{\sim}{v} = 0 = \nabla \cdot \underset{\sim}{B}$. Temporarily ignoring the dissipation, the most general linearized solutions can be written as $\underset{\sim}{B} = \underset{\sim}{b}_R + \underset{\sim}{b}_L$, $\underset{\sim}{v} = -\underset{\sim}{b}_R + \underset{\sim}{b}_L$, where

$$\begin{aligned} \underset{\sim}{b}_R &= \Sigma_{\underset{\sim}{k}} \, \underset{\sim}{b}^R_{\underset{\sim}{k}} \exp(i\underset{\sim}{k} \cdot \underset{\sim}{x} - i\omega(\underset{\sim}{k})t) + \text{c.c.} \\ \underset{\sim}{b}_L &= \Sigma_{\underset{\sim}{k}} \, \underset{\sim}{b}^L_{\underset{\sim}{k}} \exp(i\underset{\sim}{k} \cdot \underset{\sim}{x} + i\omega(\underset{\sim}{k})t) + \text{c.c.} \end{aligned} \tag{9}$$

with $\omega(\underset{\sim}{k}) = \underset{\sim}{k} \cdot \underset{\sim}{B}_o$, "c.c." stands for complex conjugate, and the amplitudes $\underset{\sim}{b}^{R,L}_{\underset{\sim}{k}}$ satisfy $\underset{\sim}{k} \cdot \underset{\sim}{b}^{R,L}_{\underset{\sim}{k}} = 0$, but are otherwise arbitrary. The division of the fields, of course, is into right and left traveling waves.

Assuming that eqs. (9) are a satisfactory zeroth order solution to eqs. (7) and (8), we may inquire, within a perturbation-theoretic framework, about the effects of directionality on the modal transfer. We may substitute the linear solutions into the right hand sides of eqs. (7) and (8) and proceed iteratively to calculate the first nonlinear correction to the linear fields. Detailed inspection shows that there is no net coupling between the right-traveling waves with each other or the left traveling waves with each other. The only non-zero couplings are between right and left traveling waves.

To resonate effectively with a third, initially-unexcited Fourier mode, there are matching conditions on both frequency and wavenumber which must be met. These are very restrictive when it is taken into consideration that one interacting wave must be right traveling and the other left traveling. If the two waves have wavenumbers $\underset{\sim}{k}_1$, $\underset{\sim}{k}_2$ and frequencies $\omega(\underset{\sim}{k}_1)$, $-\omega(\underset{\sim}{k}_2)$, the conditions that they be able to excite a third wave resonantly with wavenumber $\underset{\sim}{k}_3$ and frequency $\pm\omega(\underset{\sim}{k}_3)$ are that

$$\underset{\sim}{k}_3 = \underset{\sim}{k}_1 + \underset{\sim}{k}_2$$

$$\pm\omega(\underset{\sim}{k}_3) = \omega(\underset{\sim}{k}_1) - \omega(\underset{\sim}{k}_2). \qquad (10)$$

Since $\omega(\underset{\sim}{k}) = \underset{\sim}{k}\cdot\underset{\sim}{B}_o$, eqs. (10) have a solution only if either $\omega(\underset{\sim}{k}_1) = 0$ or $\omega(\underset{\sim}{k}_2) = 0$, so that either $\underset{\sim}{k}_1$ or $\underset{\sim}{k}_2$ has zero component along $\underset{\sim}{B}_o$. Thus, a three-wave resonant interaction can result in the excitation of a wave with a larger value of $|\underset{\sim}{k}_y|$ than that of either of the other two, but never with a larger value of $|\underset{\sim}{k}_x|$. It is clear that excitations may readily transfer energy by this process in the perpendicular direction in $\underset{\sim}{k}$ space but not in the parallel one.

An initially isotropic distribution in $\underset{\sim}{k}$ space elongates in the perpendicular direction until something stops the migration to larger $|k_y|$. In the present computation, that is either k_d or, for the truncated non-dissipative model, k_{max}. In the latter case, eventual isotropization occurs as a consequence of higher order processes. In the presence of finite dissipative decay, the anisotropy persists, as in Fig. 10.

We believe the above-described mechanism to be responsible for the observed anisotropy of magnetic fluctuations in toroidal devices. For a given level of excitations, k_d increases as ν and η decrease, so the effect

should be most pronounced at high Reynolds numbers. The independence of further increases in B_o, beyond a certain modest level, must simply mean that transfer in the parallel $\underset{\sim}{k}$-space direction has been effectively frozen relative to the transfer perpendicular to $\underset{\sim}{B}$ beyond a value of B_o just a few times the mean fluctuating field strength.

The natural directions into which these investigations should be taken are to some degree obvious. First, considerably higher Reynolds numbers, with their necessarily higher spatial resolution, should be investigated. Second, spatially inhomogeneous vacuum fields should be added to ascertain the effects of mean field curvature on the anisotropy. Finally, the effects of the mean fields on the small scales need to be ascertained: how does $\underset{\sim}{B}_o$ affect current filamentation, x-point behavior, and magnetic re-connection?

ACKNOWLEDGMENTS

This work was supported in part by the U.S. Department of Energy and the National Aeronautics and Space Administration. One of us (W.H.M.) wishes to acknowledge support as a National Academy of Sciences/ National Research Council Postdoctoral Fellow.

REFERENCES

FYFE, D. & MONTGOMERY, D. 1976 J. Plasma Phys. 16, 181.

FYFE, D., JOYCE, G., & MONTGOMERY, D. 1977a J. Plasma Phys. 17, 317.

FYFE, D. MONTGOMERY, D., & JOYCE, G. 1977b J. Plasma Phys. 17, 369.

KRAICHNAN, R. H. & MONTGOMERY, D. 1980 Rept. Prog. Phys. 43, 547.

LESLIE, D. C. 1973 Developments in the Theory of Turbulence (Oxford: Clarendon Press).

MATTHAEUS, W. H. & MONTGOMERY, D. 1980 Ann. N.Y. Acad. Sci. 357, 203 [Proc. Int. Conf. on Nonlinear Dynamics].

MATTHAEUS, W. H. & MONTGOMERY, D. 1981 J. Plasma Phys. 25, 11.

MONTGOMERY, D. 1982 "Major Disruptions, Inverse Cascades, and the Strauss Equations", to appear in Physica Scripta [Proc. Int. Conf. on Plasma Physics, Göteborg, 1982].

ORSZAG, S. A. 1971 Stud. Appl. Math. 50, 293.

ORSZAG, S. A. & TANG, C.-M. 1979 J. Fluid Mech. 90, 129.

PATTERSON, G. S. & ORSZAG, S. A. 1971 Phys. Fluids 14, 2538.

POUQUET, A. 1978 J. Fluid Mech. 88, 1.

ROBINSON, D.C., RUSBRIDGE, M. G., & SAUNDERS, P. A. H. 1968 Plasma Phys. 10, 1005.

ROBINSON, D. C. & RUSBRIDGE, M. G. 1971 Phys. Fluids 14, 2499.

RUSBRIDGE, M. G. 1969 Plasma Phys. 11, 35.

SHEBALIN, J. V. 1982 Ph.D. Thesis, William and Mary.

STRAUSS, H. R. 1976 Phys. Fluids 19, 134.

ZWEBEN, S. J., MENYUK, C. P., & TAYLOR, R. J. 1979 Phys. Rev. Lett. 42, 1270.

ZWEBEN, S. J. & TAYLOR, R. J. 1981 Nucl. Fusion 21, 193.

Table 1. Non-dissipative runs ($\nu = 0 = \eta$) for comparison with absolute equilibrium ensemble theory [Time step: $(256)^{-1}$. Total no. of time steps: 12,800. Averages taken over last 11,520 time steps.]

	Initial	Final	Time Average	% Change (Initial-Final)
		A1($B_o = 0$)		
E	1.000	0.9714	0.9782	2.9
P	0.2354	0.2167	0.2227	7.9
A	0.03288	0.03286	0.03288	0.06
		A2($B_o = 1$)		
E	1.0000	1.0150	1.0062	1.5
P	0.2354	0.2277	0.2313	3.3
A	0.03288	0.01497	0.01489	54.5

	$R = E_B/E_v$			
	Initial	Final	Time Average	Theoretical
A1	1.0000	1.0058	1.0608	1.0484
A2	1.0000	0.9825	1.0004	1.0000

Table 2. Run Parameters

Run	k_{max}	ν, η	B_o	Time Step Size	Total # of Time Steps
A1	16	0	0	1/256	12800
A2	16	0	1	1/256	12800
A3	32	.005	0	1/256	1280
A4	32	.005	1	1/256	1280
A5	32	.01	0	1/256	1280
A6	32	.01	1	1/256	1280
A7	32	.02	0	1/256	1280
A8	32	.02	1	1/256	1280
A9	16	.01	0	1/128	640
A10	16	.01	1	1/128	640
A11	16	.01	1/16	1/128	640
A12	16	.01	1/8	1/128	640
A13	16	.01	1/4	1/128	640
A14	16	.01	1/2	1/128	640
A15	16	.01	2	1/256	1280
A16	16	.01	4	1/512	2560
A17	16	.01	8	1/1024	5120
A18	16	.01	16	1/2048	10240
B1	16	0	1	1/128	3200
B2	16	.0025	1	1/128	3200

Set A: initial equipartion of energy in all magnetic and kinetic Fourier modes.

Set B: initial equipartion of energy in Fourier modes such that $9 \leq k^2 \leq 25$; Fourier modes outside this annulus initially set to zero.

Initial rms values of $|\vec{B}|^2$ and $|\vec{v}|^2$ were both equal to one for sets A and B.

Table 3. Average Angles between t = 1.5 and 5.0

ν,η	θ_ψ	θ_a	θ_v	θ_B	θ_ω	θ_J
.005	53.4	50.6	58.2	59.3	64.0	67.5
.01	51.6	48.5	54.8	55.0	60.5	64.0
.02	48.7	46.5	50.8	50.2	53.6	56.6

Table 4. Maximum Values of k_d, Ω and J for runs A3 through A8

Run	ν, η	B_o	Max k_d	Max Ω	Max J
A3	.005	0	49.6	25.0	51.8
A4	.005	1	48.3	30.6	38.0
A5	.01	0	32.2	17.0	39.0
A6	.01	1	31.4	21.4	27.8
A7	.02	0	21.0	17.0	26.8
A8	.02	1	20.8	17.0	20.3

FIGURE CAPTIONS

Fig. 1. Directionally averaged kinetic energy spectra for run A1: $B_o = 0$, $\nu = \eta = 0$, $k_{max} = 16$. Solid line is theoretical prediction.

Fig. 2. Directionally averaged magnetic energy spectra for run A1: $B_o = 0$, $\nu = \eta = 0$, $k_{max} = 16$. Solid line is theoretical prediction.

Fig. 3. Directionally averaged kinetic energy spectra for run A2: $B_o = 1$, $\nu = \eta = 0$, $k_{max} = 16$. Solid line is theoretical prediction.

Fig. 4. Directionally averaged magretic energy spectra for run A2: $B_o = 1$, $\nu = \eta = 0$, $k_{max} = 16$. Solid line is theoretical prediction.

Fig. 5. The quantities E, P, A, and R for run A5: $B_o = 0$, $\nu = \eta = 0.01$, $k_{max} = 32$.

Fig. 6. The quantities E, P, A, and R for run A6: $B_o = 1$, $\nu = \eta = 0.01$, $k_{max} = 32$.

Fig. 7. Measures of anisotropy for run A5: $B_o = 0$, $\nu = \eta = 0.01$, $k_{max} = 32$.

Fig. 8. Measures of anisotropy for run A6: $B_o = 1$, $\nu = \eta = 0.01$, $k_{max} = 32$.

Fig. 9. a) Dissipation wave number for run A5; b) dissipation wave number for run A6; c) mean square vorticity for run A5; d) mean square current for run A5; e) mean square vorticity for run A6; f) mean square current for run A6.

Fig. 10. The angles θ_v and θ_B for runs B1 ($B_o = 1$, $\nu = \eta = 0$) and B2 ($B_o = 1$, $\nu = \eta = 0.0025$).

Fig. 11. Measures of anisotropy as a function of mean field strength B_o.

Fig. 12. a) Maximum k_d as a function of B_o; b) time of max k_d; c) maximum mean square vorticity as a function of B_o; d) maximum mean square current as a function of B_o.

Fig. 13. a) Vorticity of set A at t = 0; b) current of set A at t = 0; c) vorticity of run A9 ($B_o = 0$, $\nu = \eta = .01$, $k_{max} = 16$) at t = 2.0; d) current of run A9 at t = 0; e) vorticity of run A15 ($B_o = 2$, $\nu = \eta = .01$, $k_{max} = 16$) at t = 2.0; f) current of run A15 at t = 2.0.

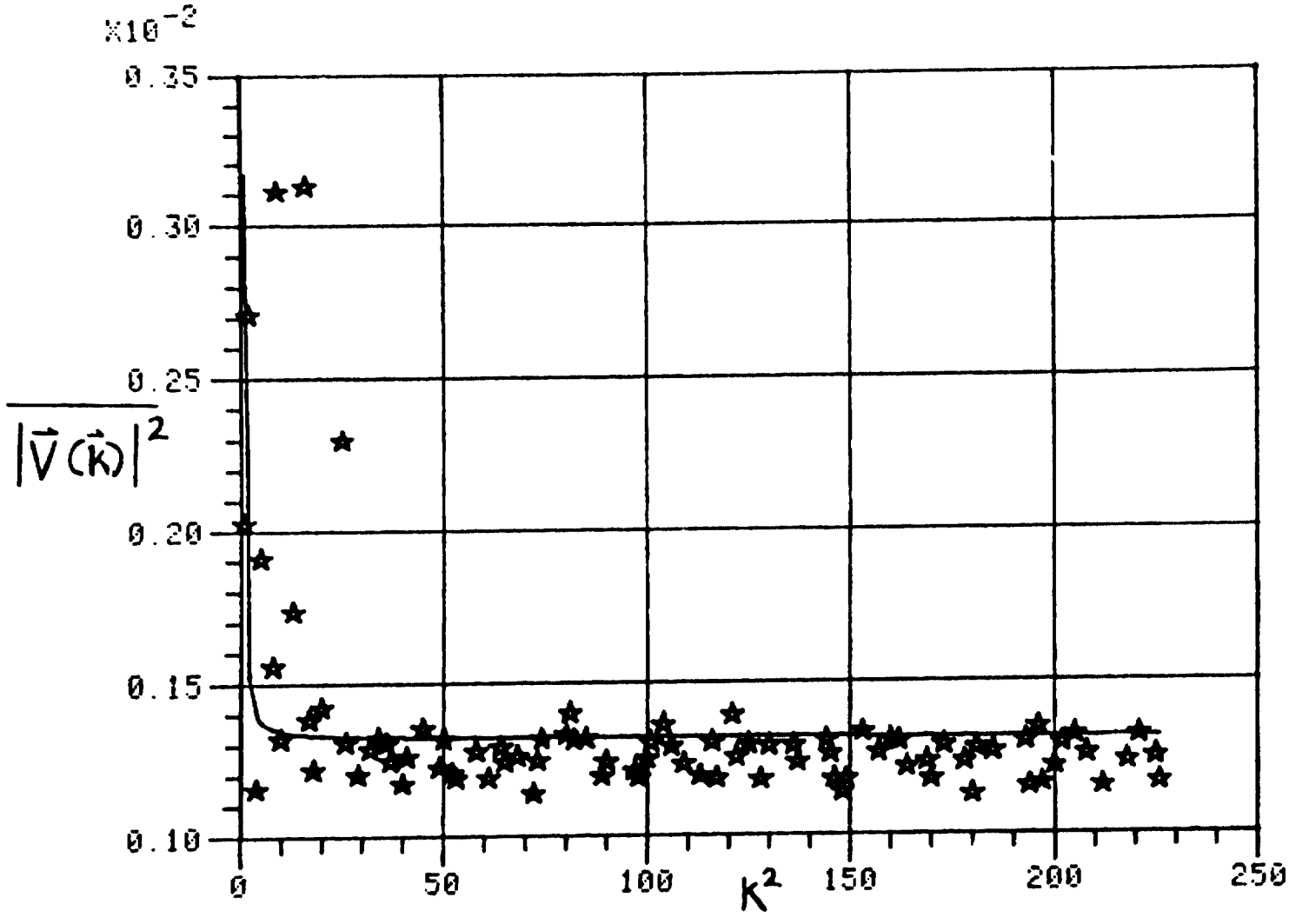

Fig. 1. Directionally averaged kinetic energy spectra for run A1:

$B_o = 0$, $\nu = \eta = 0$, $k_{max} = 16$. Solid line is theoretical prediction.

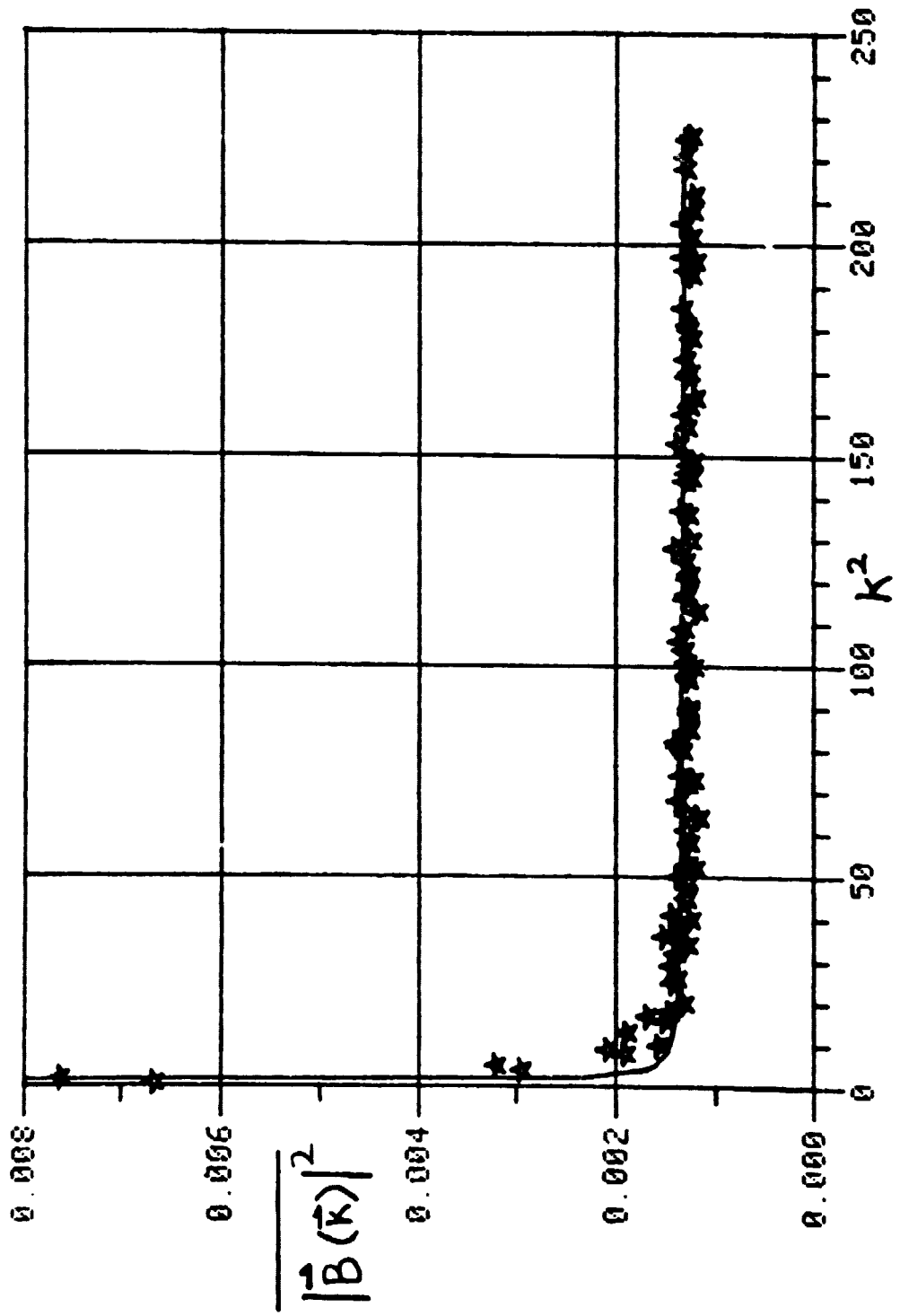

Fig. 2. Directionally averaged magnetic energy spectra for run A1:

$B_o = 0$, $\nu = \eta = 0$, $k_{max} = 16$. Solid line is theoretical prediction.

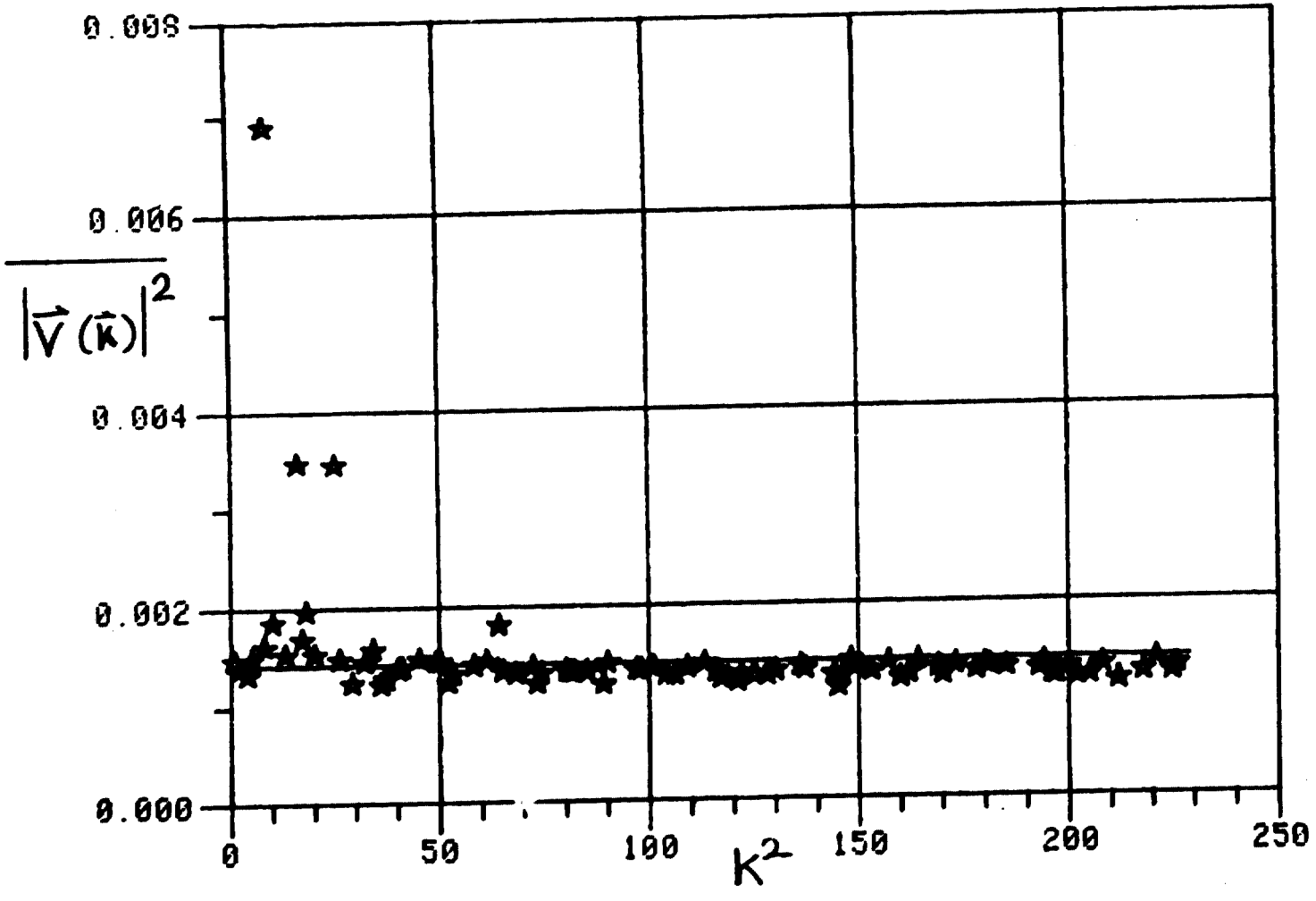

Fig. 3. Directionally averaged kinetic energy spectra for run A2: $B_o = 1$, $\nu = \eta = 0$, $k_{max} = 16$. Solid line is theoretical prediction.

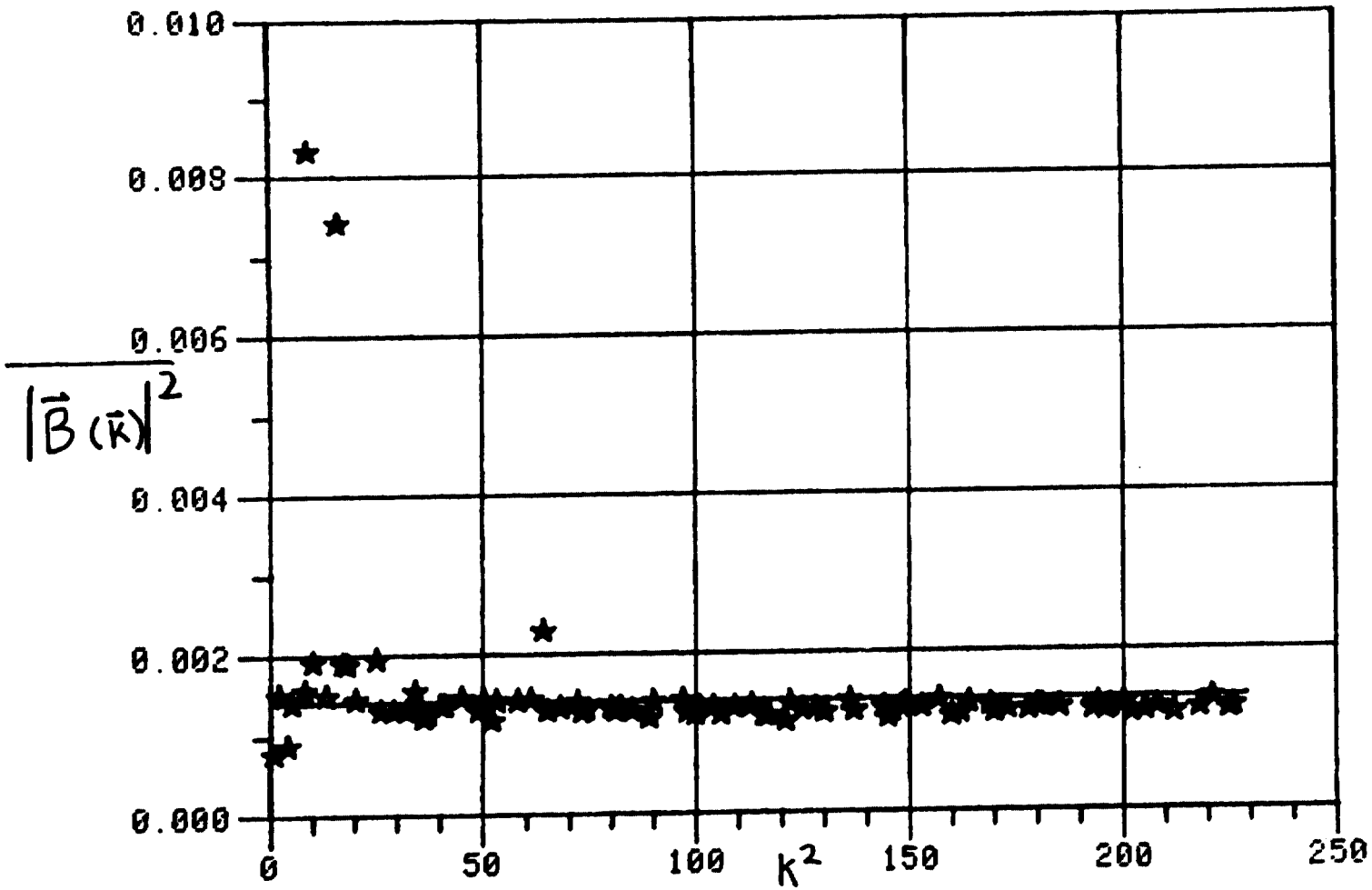

Fig. 4. Directionally averaged magnetic energy spectra for run A2: $B_o = 1$, $\nu = \eta = 0$, $k_{max} = 16$. Solid line is theoretical prediction.

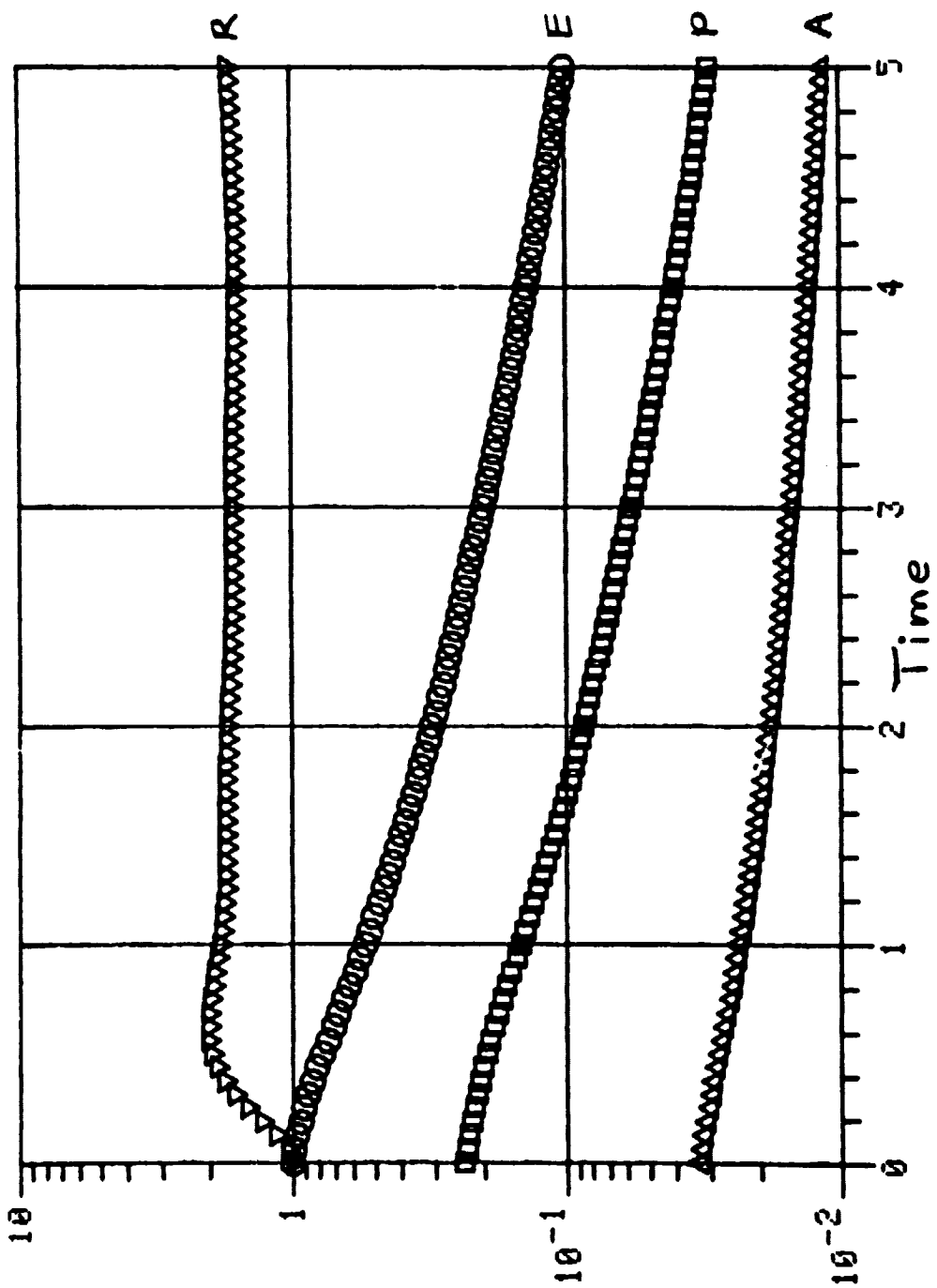

Fig. 5. The quantities E, P, A, and R for run A5: $B_o = 0$, $\nu = \eta = 0.01$, $k_{max} = 32$.

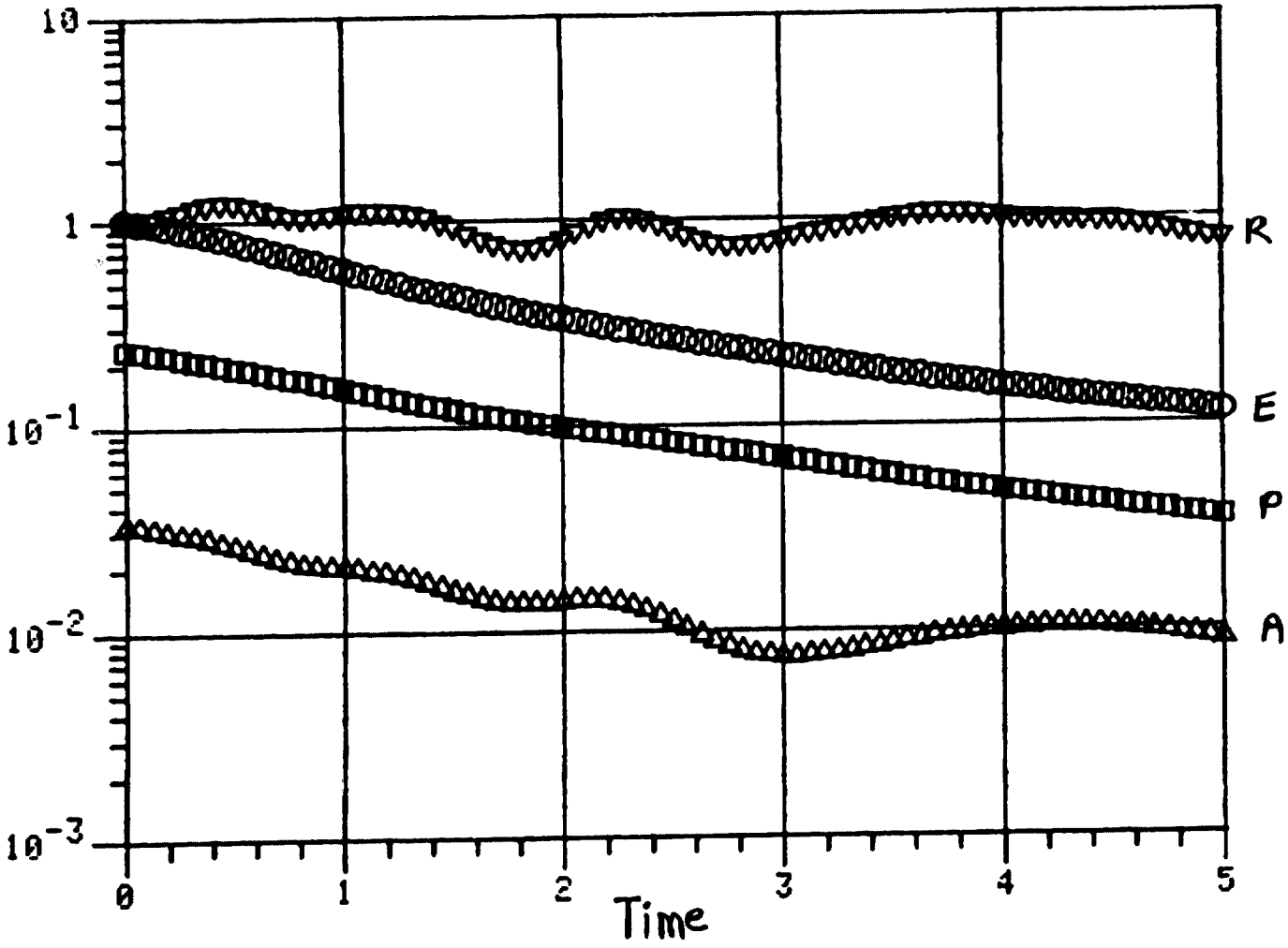

Fig. 6. The quantities E, P, A, and R for run A6: $B_o = 1$, $\nu = \eta = 0.01$, $k_{max} = 32$.

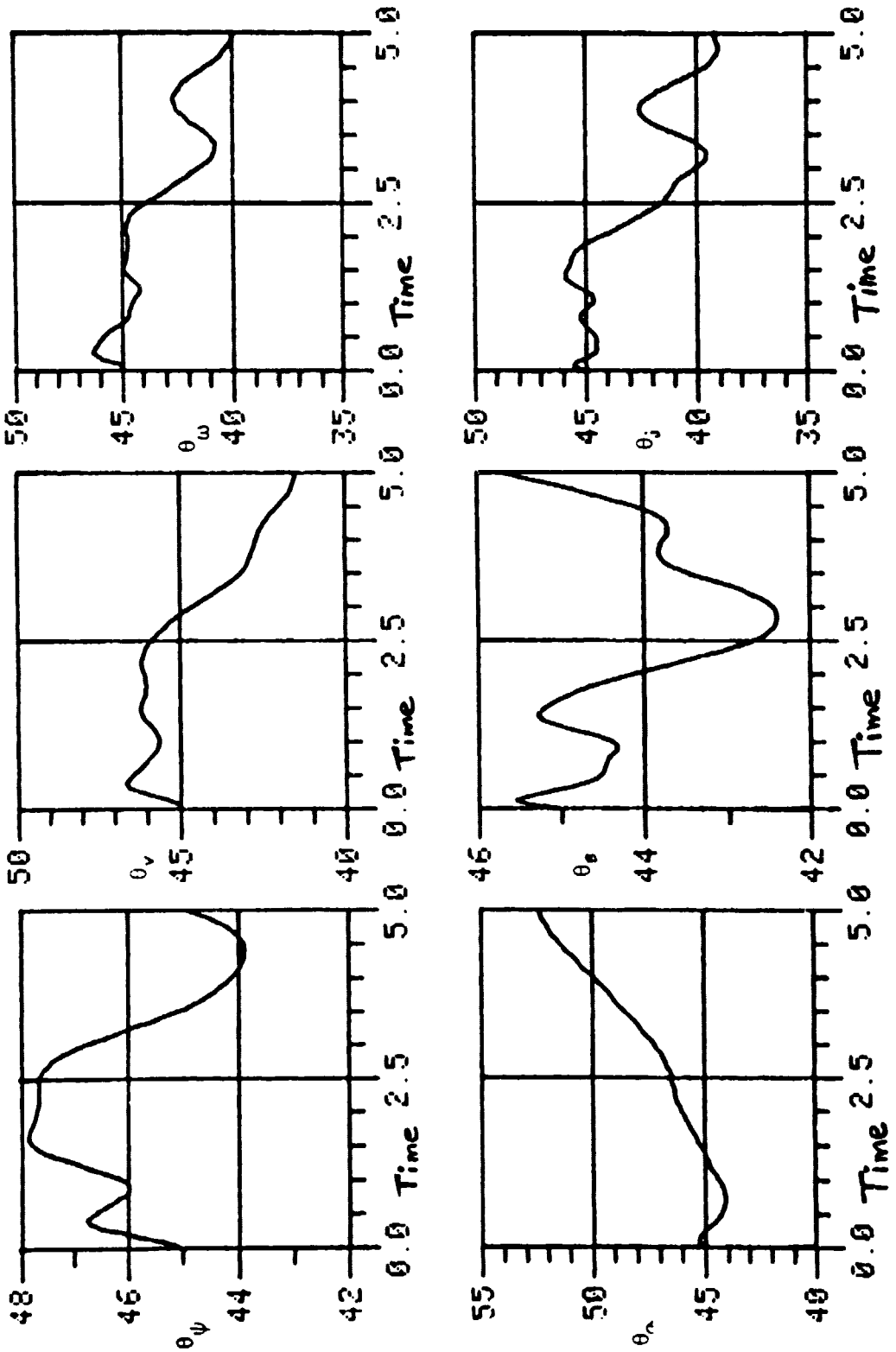

Fig. 7. Measures of anisotropy for run A5: $B_o = 0$, $\nu = \eta = 0.01$, $k_{max} = 32$.

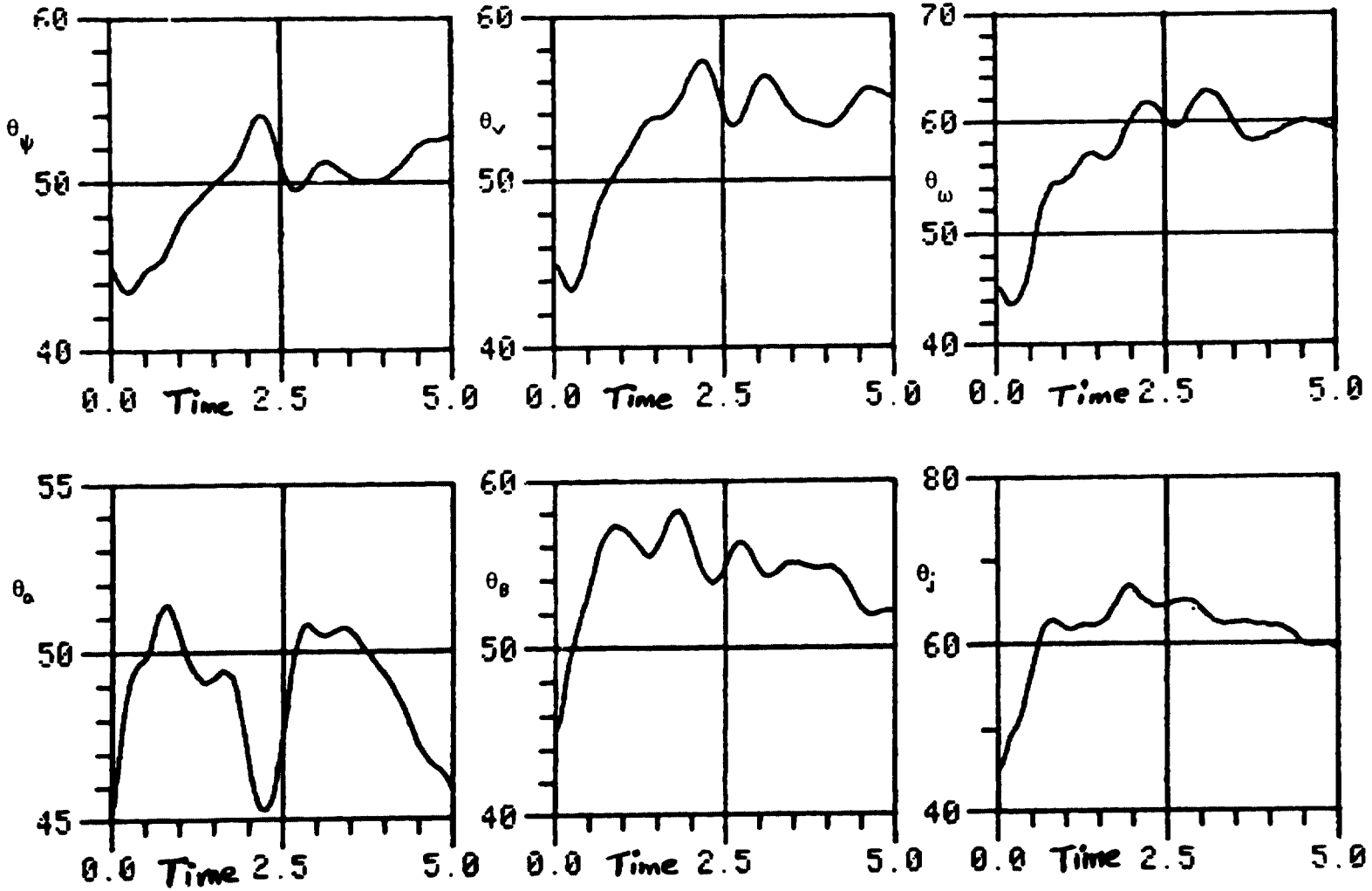

Fig. 8. Measures of anisotropy for run A6: $B_o = 1$, $\nu = \eta = 0.01$, $k_{max} = 32$.

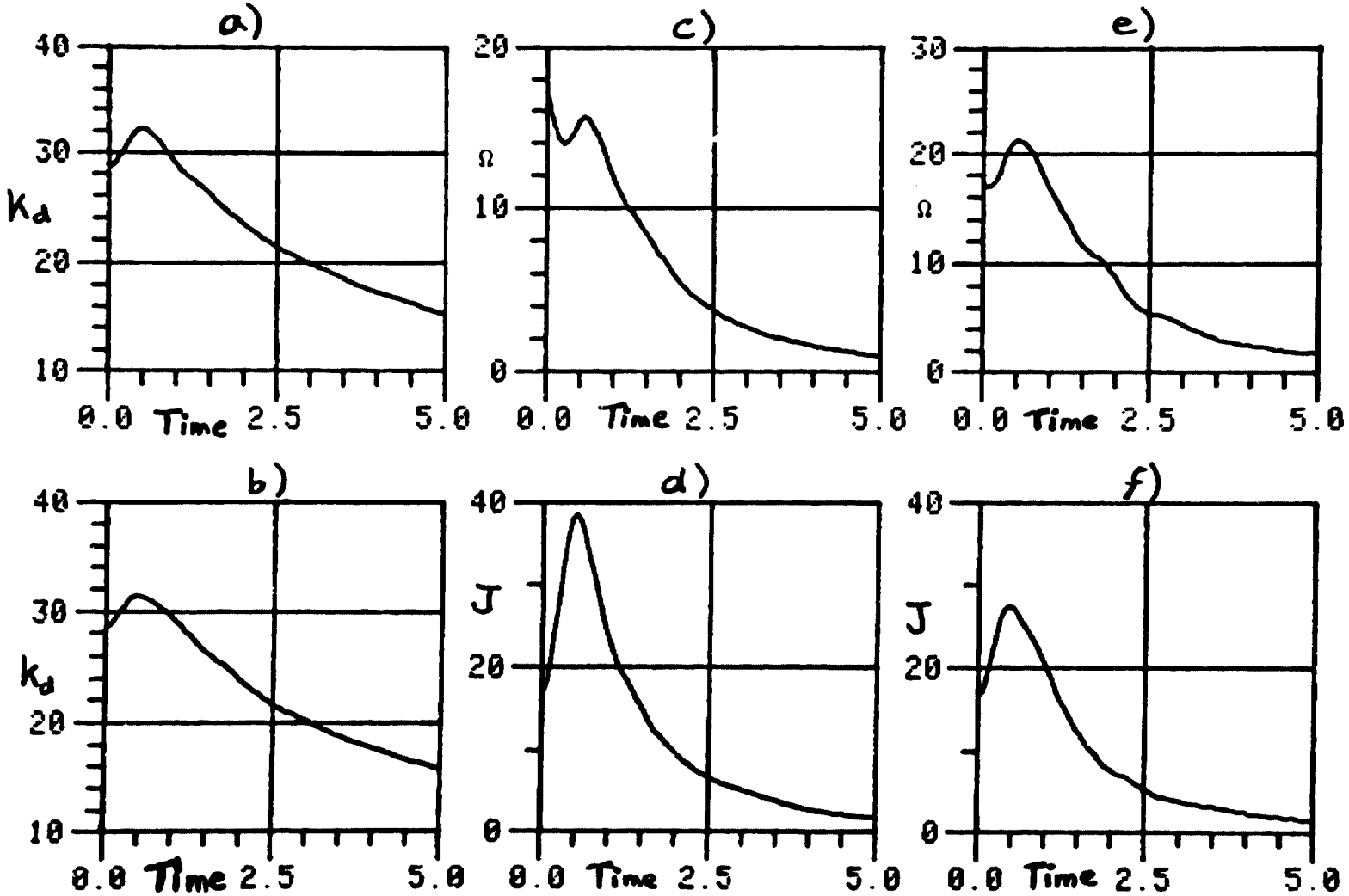

Fig. 9. a) Dissipation wave number for run A5; b) dissipation wave number for run A6; c) mean square vorticity for run A5; d) mean square current for run A5; e) mean square vorticity for run A6; f) mean square current for run A6.

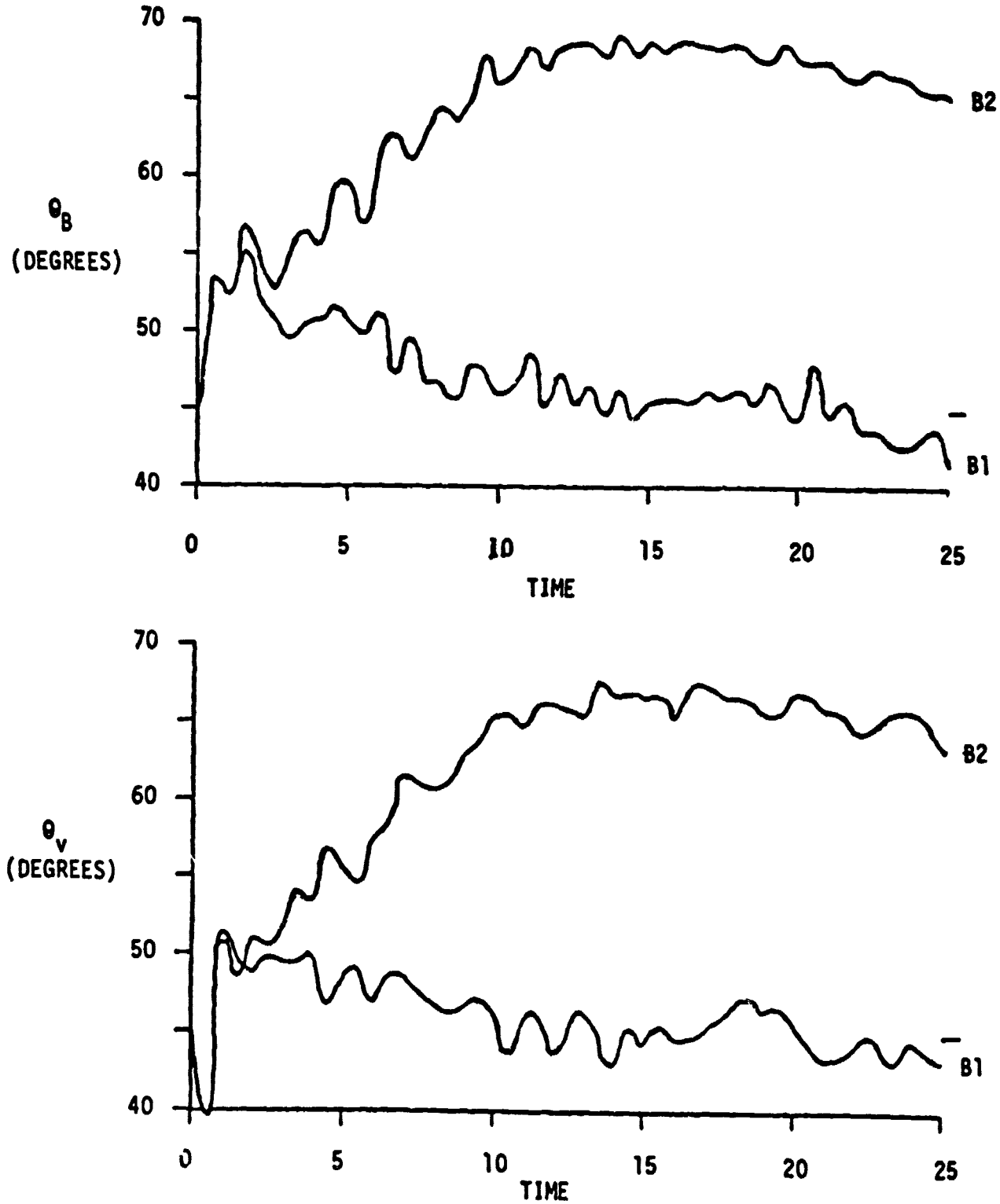

Fig. 10. The angles θ_v and θ_B for runs B1 ($B_o = 1$, $\nu = \eta = 0$) and B2 ($B_o = 1$, $\nu = \eta = 0.0025$).

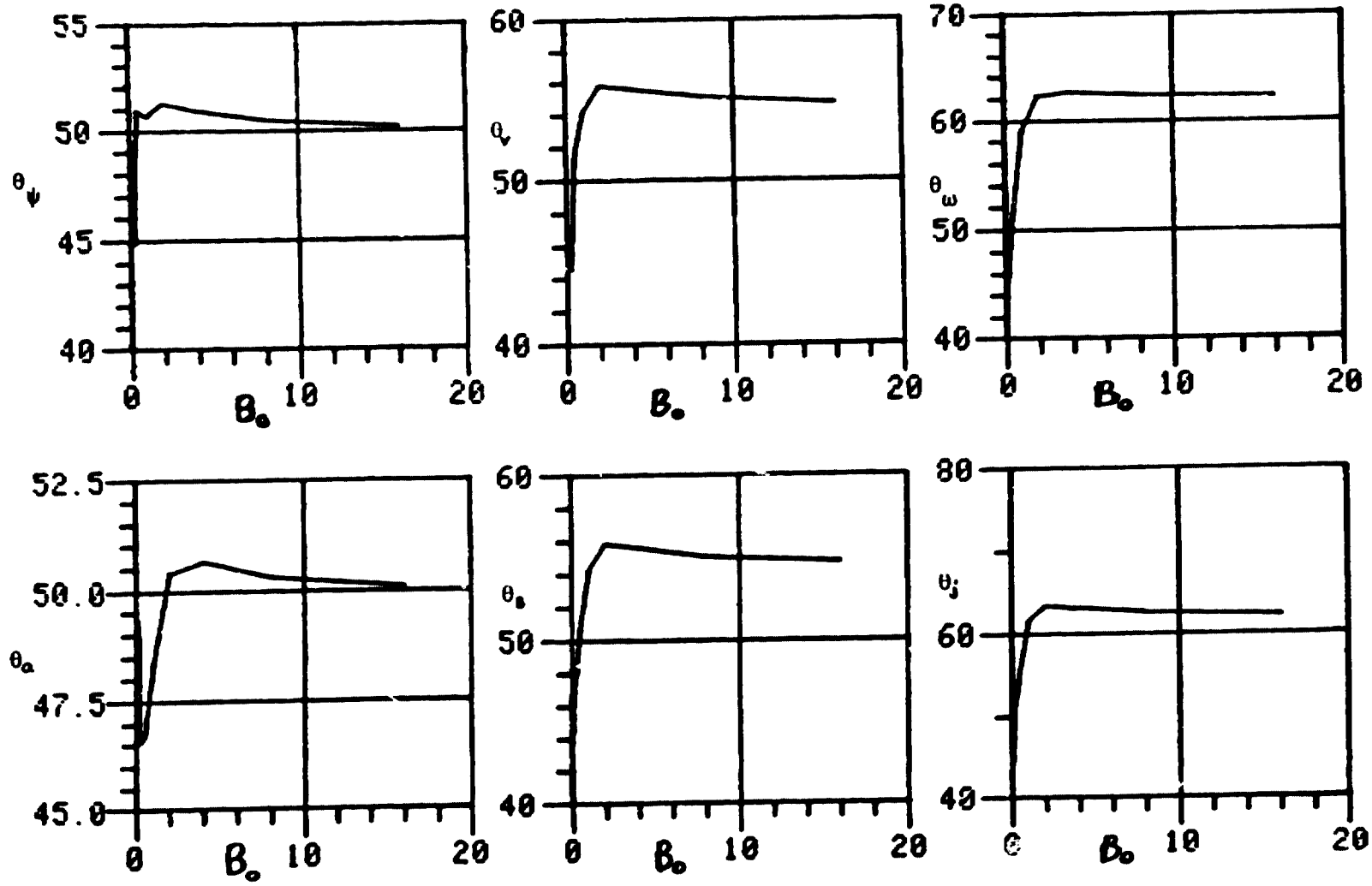

Fig. 11. Measures of anisotropy as a function of mean field strength B_o.

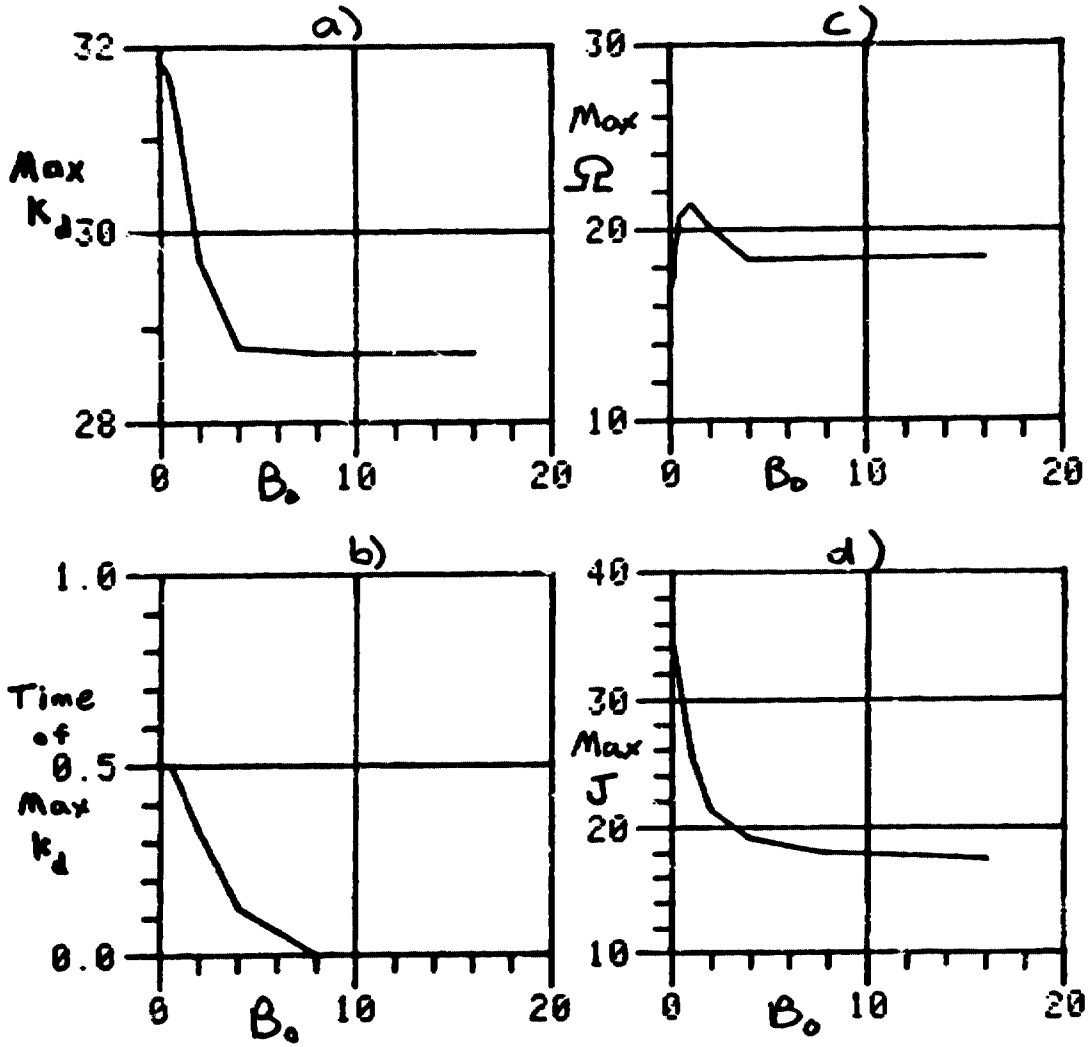

Fig. 12. a) Maximum k_d as a function of B_o; b) time of max k_d; c) maximum mean square vorticity as a function of B_o; d) maximum mean square current as a function of B_o.

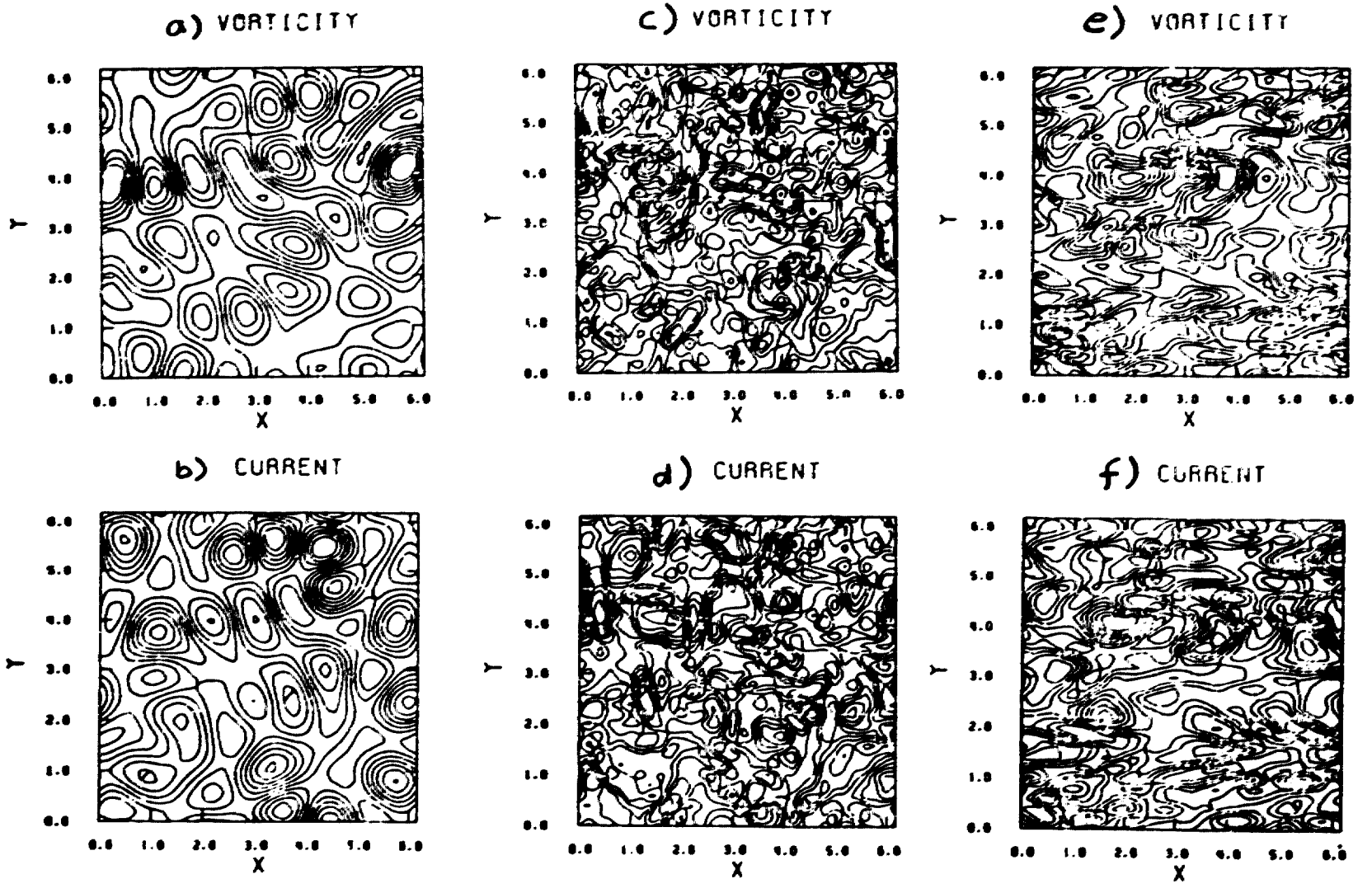

Fig. 13. a) Vorticity of set A at t = 0; b) current of set A at t = 0; c) vorticity of run A9 (B_o = 0, $\nu = \eta$ = .01, k_{max} = 16) at t = 2.0; d) current of run A9 at t = 0; e) vorticity of run A15 (B_o = 2, $\nu = \eta$ = .01, k_{max} = 16) at t = 2.0; f) current of run A15 at t = 2.0.